# Geometric and kinematic model of bed length balanced graben structures

By Peter Keller[1])

ABSTRACT

Graben tectonics are investigated under the assumption of bed length conservation during deformation. In order to balance hanging-wall bed length, a new deformation model for half-grabens with listric master fault is proposed. The model requires full-grabens and normal faults to segment the hanging-wall. These structures do not contribute to regional extension and are considered as *secondary structures*. They are formed by simple shear and deformation is limited in depth. Therefore they are referred to as *blind normal faults* and *blind grabens*. A mathematical relationship between the geometry of half-grabens and secondary structures is described as a function of the listric fault shape.

As a kinematic consequence of the model the secondary structures migrate towards the cut-off of the listric fault into higher stratigraphic levels. The application of the geometric relationships to seismic data confirms the model to geological systems.

ZUSAMMENFASSUNG

Ein Modell zur Beschreibung der Deformation von Halb-Gräben mit listrischer Abscherung unter Erhaltung von Schichtlänge und Schichtdicke wird diskutiert. Das Modell verlangt Gräben und Verwerfungen, die das Hangende des Halb-Grabens segmentieren. Diese Strukturen liefern keinen Beitrag zur regionalen Extension und werden deshalb als *Sekundär-Strukturen* bezeichnet. Ein neuer Mechanismus der einfachen Scherung zur Bildung dieser Strukturen wird vorgestellt. Aus diesem Mechanismus resultiert eine Begrenzung der Sekundär-Strukturen in bestimmter Tiefe, daher werden sie *Blinde Gräben* und *Blinde Verwerfungen* genannt. Eine mathematische Beziehung zwischen der Halb-Graben Geometrie und den Sekundär-Strukturen als Funktion des listrischen Bruches wird hergeleitet.

Mit fortschreitender Extension migrieren die Sekundär-Strukturen in Richtung des Abriss des listrischen Bruches und in höhere Niveaus. Mit der Anwendung der hergeleiteten Beziehungen auf seismische Linien wird das Modell für geologische Systeme bestätigt.

## Introduction

Crustal extension is highly variable in terms of deformation style. Different models based on seismic data, analogue experiments or cross-section balancing methods have been developed to explain extensional structures. Two groups of models can be deduced from literature. The first group considers extension as interaction of two layers, with brittle deformation in the upper one and ductile deformation in the lower one (Brun et al. 1985; Eaton 1982; Faugere & Brun 1984; Klemperer 1988; Prof-

---

[1]) Institut für Geophysik, ETH-Hönggerberg, CH–8093 Zürich, Switzerland.

FETT 1977; VENDEVILLE et al. 1987). In these models the ductile layer is the lower continental crust (DE CHARPAL et al. 1978; LE PICHON & SIBUET 1983) or on a smaller scale evaporitic deposits (ROWAN & KLIGFIELD 1989). In the upper layer rigid block deformation along listric and/or planar normal faults is the dominant deformation style (FAURE & CHERMETTE 1989; JACKSON et al. 1982; WERNICKE & BURCHFIELD 1982). In the lower layer the discrete deformation of normal faults is absorbed by ductile or penetrative deformation (COBBOLD 1983; VENDEVILLE et al. 1987). There is no detachment between the two layers.

In contrast the second group of models postulates a lowermost detachment surface on which extension takes place (BALLY et al. 1981; GANS et al. 1985; GIBBS 1984; WERNICKE & BURCHFIELD 1982). From this detachment normal faults cut upwards to the surface. This configuration leads to half-graben structures (BALLY 1982; ROSEN-DAHL 1987). Half-grabens are characterized by a steep edge and a shallow dipping end. The steep edge is caused by a listric or planar normal fault. During extension the foot wall stays undeformed whereas the hanging-wall becomes deformed by reverse drags, normal faults, synthetic or antithetic to the listric fault, and full-grabens.

The aim of this work is to analyze geometry and kinematics of extensional tectonics above a lowermost detachment surface by using bed length balancing techniques. New models and geometric algorithms are proposed for the formation of half-grabens, grabens and normal faults. Kinematics of half-graben deformation are analyzed by stepwise forward construction of synthetic cross-sections. The proposed model is compared to structures in extensional terrains and tested versus seismic data and laboratory experiments.

## Geometric relations of hanging-wall deformation

Cross-section balancing techniques have been developed to analyze geometry and kinematics in areas of contractional tectonics. They have been applied successfully in interpreting many thrust belts (BOYER & ELLIOT 1982; LAUBSCHER 1965; SUPPE 1983; GEISER 1988). Some of these balancing techniques have been expanded to extensional tectonics. The balancing of extensional structures, such as grabens and hanging-wall geometries above steep normal faults, leads to a void between the foot wall and the hanging-wall. The space problem has been resolved by the use of different geometric algorithms which are related to specific deformation mechanisms. GIBBS (1984) and GROSHONG (1989) solve the space problem by reverse-drag folding and thinning of hanging-wall layers. WERNICKE & BURCHFIELD (1982) alternatively have proposed a model of rotating blocks (domino structure) to balance extensional structures by preserving bed length and thickness. In there model empty space results between the rotating blocks and the foot wall, thus cross-section area is not preserved. Other models, however, have suggested simple-shear mechanisms to resolve the space problem. In the graphical models of VERALL (1981) and GIBBS (1983, 1984) the shear is restricted to vertical planes, whereas the mathematical model of WHITE et al. (1986) takes simple-shear movement in any designated direction into consideration.

*Geometric assumptions* – The geometric analyses of hanging-wall deformation are based on the assumption, that a section has to be balanced geometrically and kinematically admissible. Thus cross-section area and bed thickness normal to bedding must be

preserved geometrically during deformation. In addition it must be possible to deform a restored section (or restore a deformed section) until the observed geometry is reached, while each intermediate deformation step has to be geometrically balanced as well. Deformation has to be parallel to the cross-section plane. The restriction of bed thickness conservation implies a deformation mechanism during folding by layer parallel slip (flexural slip). Furthermore, deformation by cleavage or ductile deformation are not allowed in the models presented.

For the construction of the section and the calculations based thereon, the kink method (cf. SUPPE 1985) is adopted, which approximates folds by straight fold limbs and curved faults by straight fault-segments. To maintain the conservation of bed thickness the axial surface of the fold has to bisect the angle between the two fold limbs. The angle between a fold limb and the axial surface defines the fold geometry and is called the "axial angle $\gamma$" (SUPPE 1983).

*Hanging-wall deformation* – The geometric elements of a half-graben used in the following calculations are shown in figure 1. The listric master fault shape is approximated by several fault-segments which are characterized by their dip to bedding ($\alpha_n$). The related hanging-wall glides by the amount *e* on this detachment and deforms as a consequence of the movement over the kinked shape of the listric fault. Four layer packages (Fig. 1: block A to D) are distinguished in relation to their movement on the listric fault. Block A glides from the lower fault-segment ($\alpha_1$) onto the flat detachment horizon. Due to this movement a gap opens between the foot wall and the hanging-wall which is closed by folding down the hanging-wall layers. This new geometric configuration is described as "roll-over anticline" or "reverse drag" (POWELL 1875, ref. HAMBLIN 1965). Block B glides on the lower fault-segment and is folded only due to the deformation in block A. Block C glides from the upper fault-segment ($\alpha_2$) onto the lower one ($\alpha_1$). This geometric configuration cannot be balanced by a reverse drag alone. Therefore layer parallel shear referred to as *hanging-wall shear* has to be introduced to balance the geometry. Block D behaves similarly to block B.
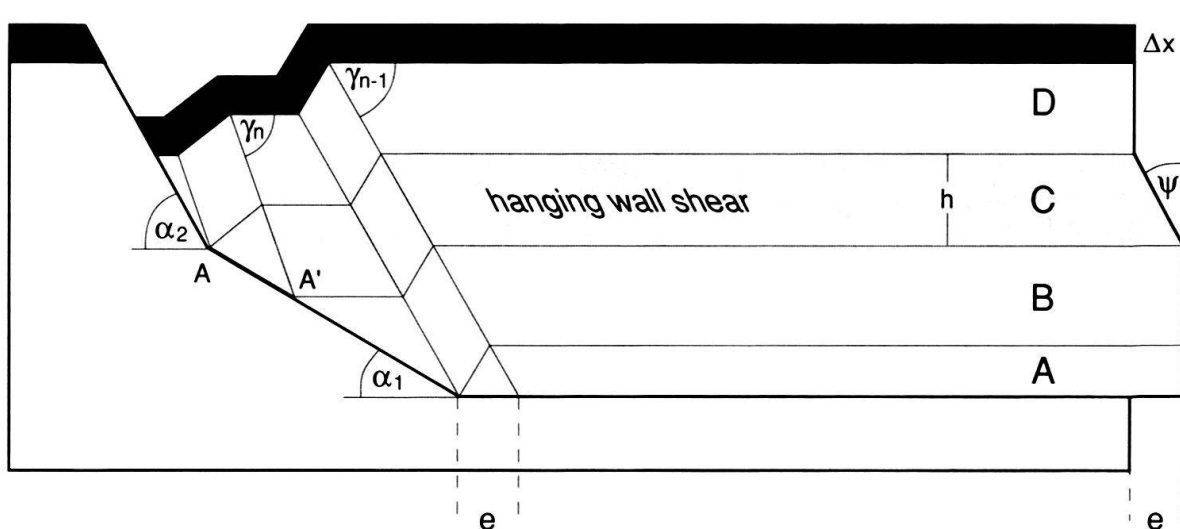


Fig. 1. Balanced geometry of half-graben structure with listric normal fault and associated reverse drag.

The hanging-wall shear $(S)$ of block C can be defined as:

$$S = \frac{\Delta x}{h} = \tan \varphi = f\,(\alpha_n, \alpha_{n-1}, \gamma) \tag{1}$$

Here $h$ is the thickness of the package of layers which is displaced from one fault-segment to a lower segment ($A \rightarrow A'$ on Fig. 1, stippled area) and $\Delta x$ is the amount of layer parallel slip at the top of this package. Furthermore, the hanging-wall shear $(S)$ is a function of the change in fault dip ($\alpha_n$, $\alpha_{n-1}$) and the reverse drag shape ($\gamma$).

*Geometric derivation of the hanging-wall shear* – The layer parallel slip $\Delta x$ can be expressed as the difference between the necessary bed length to fill the gap by reverse drag folding ($a$) and the given bed length ($b$) (Fig. 2)

$$\Delta x = a - b \tag{2}$$

The bed length $a$ and $b$ are expressed in eq (2a) and eq (2b) respectively

$$a = \frac{h}{\sin 2\gamma} \cdot \left( 1 - \frac{\sin \alpha_{n-1}}{\sin (2\gamma - \alpha_{n-1})} \right) \tag{2a}$$

$$b = h \cdot (\cot \alpha_n - \cot \gamma) \tag{2b}$$

Inserting eq (2a) and eq (2b) in eq (2) and dividing by $h$ leads to eq (3).

$$S = \frac{\Delta x}{h} = \frac{1}{\sin 2\gamma} \cdot \left( 1 - \frac{\sin \alpha_{n-1}}{\sin [2\gamma - \alpha_{n-1}]} \right) - \cot \alpha_n + \cot \gamma \tag{3}$$
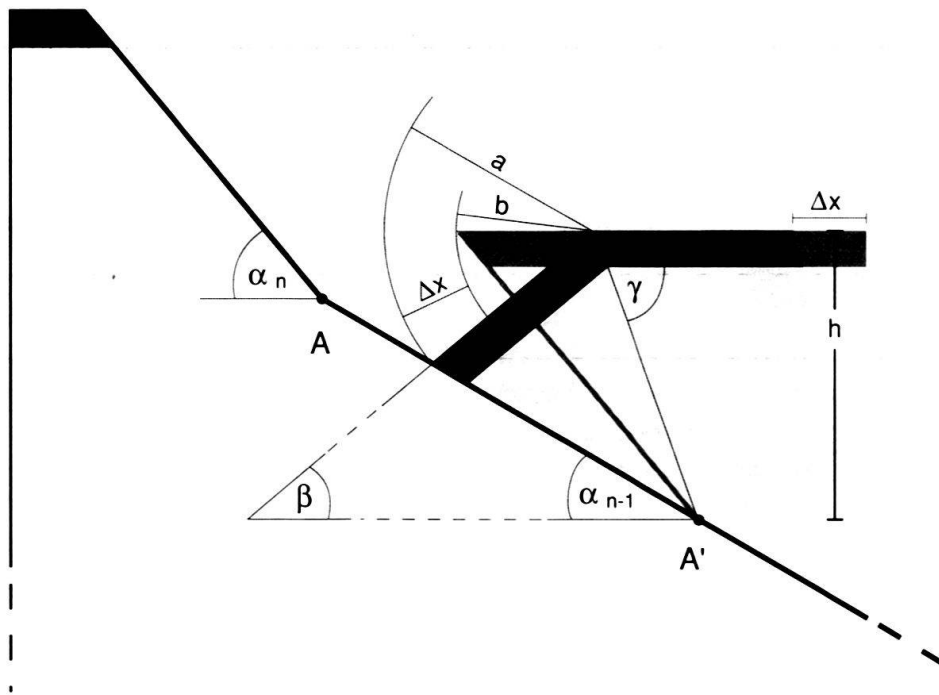


Fig. 2. Geometric relationship used to derive the function of the hanging-wall shear ($S = \Delta x/h$), the axial angle ($\gamma$) and the listric fault shape ($\alpha_1$, $\alpha_2$) (eq 3).

The change in bed dip due to reverse drag folding is expressed by the angle $\beta$ defined in eq (4).

$$\beta = 180 - 2\gamma \tag{4}$$

Equation (3) is a trigonometric expression of the hanging-wall shear $(S)$. $S$ is a function of the three variables $\alpha_n$, $\alpha_{n-1}$ and $\gamma$. For a unique solution of the function additional restrictions have to be found which reduce the variables. A similar geometric relation for contractional tectonics is discussed by SUPPE (1983, Fig. 17, eq 31). To receive a unique solution for the hanging-wall geometry SUPPE (1983) defined the shear as zero $(S = 0)$. A consequence of this restriction is, that dips of fault-segments $(\alpha_n)$ steeper than 30° are not allowed.

An additional restriction for steep normal faults $(\alpha > 30°)$ is deduced to receive unique solutions for eq (3). Graphic solutions of this equation for $\alpha_n$ = constant are shown in Figure 3. Distinction can be made between a positive/negative or a zero value for $S$. The prefix indicates different direction of shear. Positive shear is defined to be opposite to the extension direction. The zero solutions are identical to SUPPE's (1983) fault bend fold solutions. For a defined pair of fault-segments $(\alpha_n, \alpha_{n-1})$ the corresponding $S$ can be varied by varying the reverse drag shape $(\gamma)$. For listric faults $(\alpha_n \geq \alpha_{n-1})$ with negative $S$, two zero solutions can be determined by varying $\gamma$ (Fig. 3). Fault-segment configurations which cause only positive $S$ show no zero solutions. By continually flattening of the lower fault-segment $(\alpha_{n-1})$ the two zero solutions move closer together. The last fault-segment configuration showing a zero solution (Fig. 3a: $\alpha_{n-1} = 0°$, $\gamma = 60°$; Fig. 3b: $\alpha_{n-1} = 25°$, $\gamma = 68.5°$; Fig. 3c: $\alpha_{n-1} = 57°$, $\gamma = 79°$; Fig. 3d: $\alpha_{n-1} = 90°$, $\gamma = 90°$) is equivalent to the minimal solution of equation (3). Geologically it seems reasonable to keep the shear $(S)$ as small as possible. Therefore zero solutions for reverse drag geometries are preferred. If zero solutions are not possible, the solution for minimal hanging-wall shear $(S_{min})$ is used to determine the reverse drag shape $(\gamma)$. The curves of $S_{min}$ in Figure 3 are plotted for all fault-segment configurations in Figure 4.

With the constraint that $S$ has to be zero or minimal, unique solutions for eq (3) are obtained. For example if $\alpha_n$ is 60° steep and $\alpha_{n-1}$ is 40° steep $\gamma$ has to be 73° and $S_{min}$ 0.32 (or: $\alpha_n = 80°$, $\alpha_{n-1} = 30° \rightarrow S_{min} = 0.92$). A range of minimal hanging-wall shear between 0.3 and 1.0 seems to correspond to reasonable listric fault shapes (cf. Fig. 4).

## Secondary structures

In the following extensional structures are proposed to compensate the required hanging-wall shear $(S_{min})$. Because $S_{min}$ is a result of the listric fault geometry also the compensating structures are induced by this master fault. Therefore they are referred to as *secondary structures*. The criteria for secondary structures are; i) one or several structures together must have the same, but oppositely directed shear profile, as required by eq (3):

$$S_{hanging-wall} = -(S_1 + S_2 + \ldots\ldots + S_i) = -S_{secondary} \tag{5}$$

ii) they have to be balanced following the above restrictions, and iii) they have to correspond to typical extensional structures. Two structures, which fulfill the above criteria are proposed in the following paragraphs.
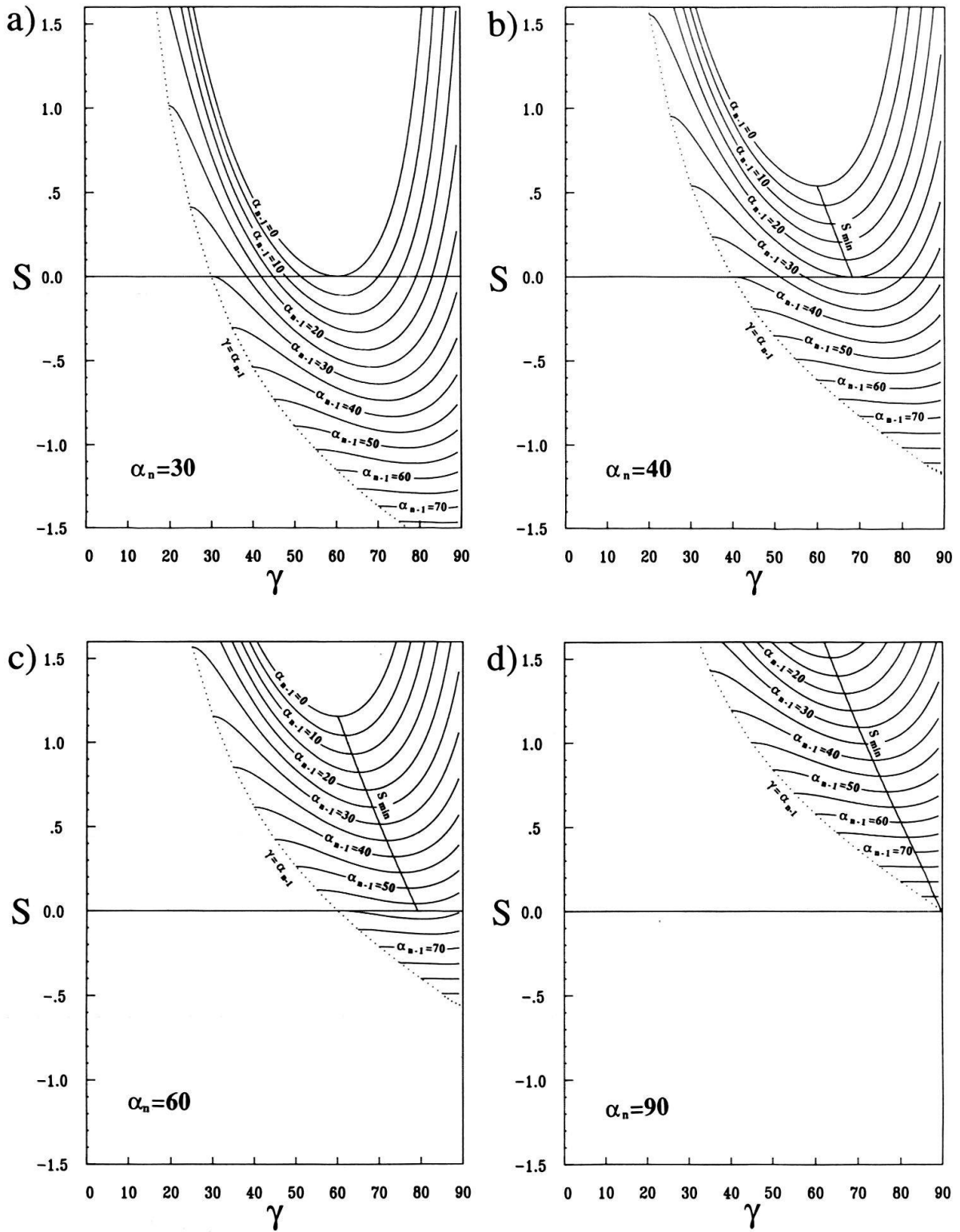
Fig. 3. Graphs of relationship between reverse drag shape ($\gamma$), dip of lower fault-segment ($\alpha_{n-1}$) and the hanging-wall shear ($S$) with constant upper fault-segment dips ($\alpha_n$).
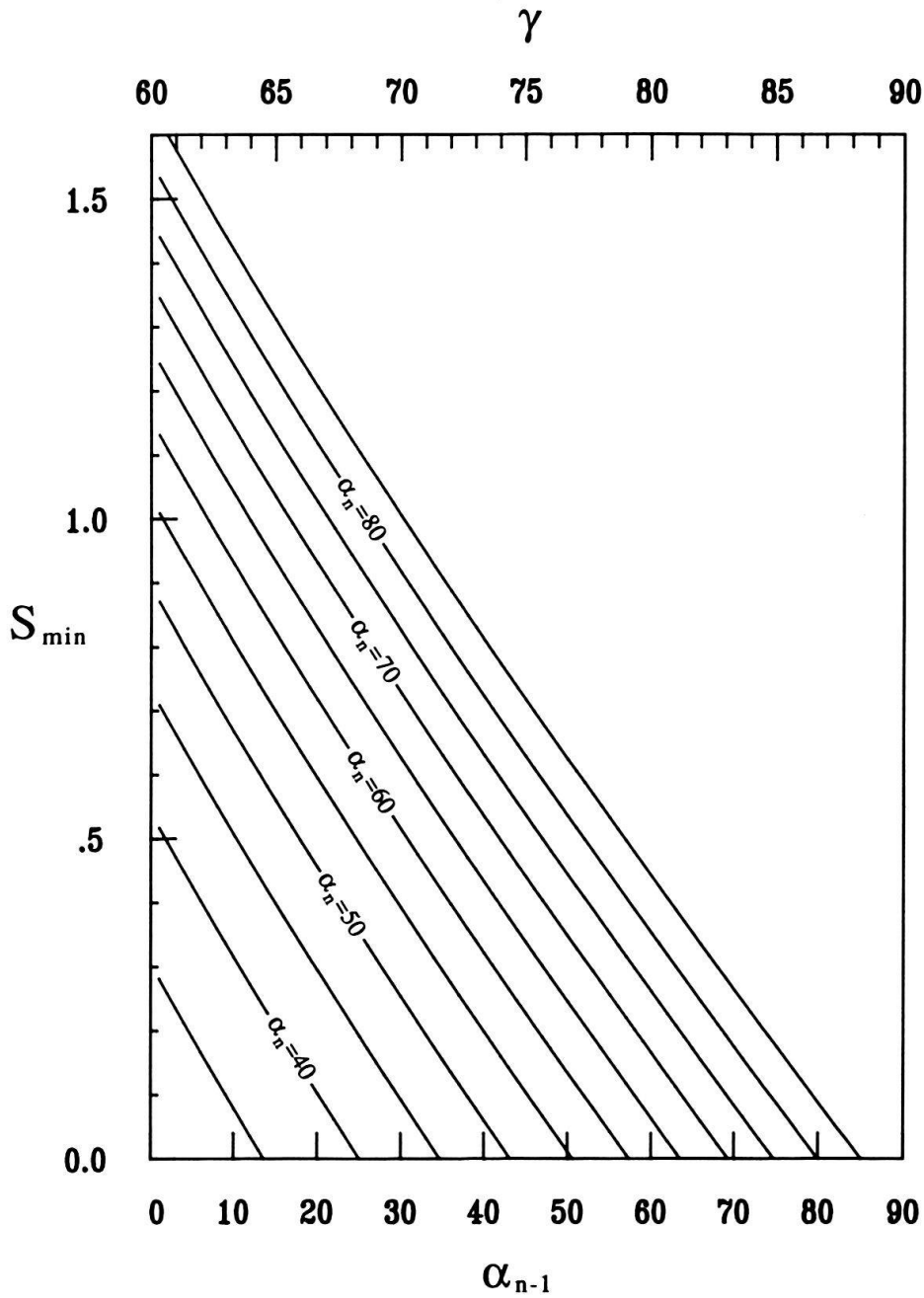
Fig. 4. Graph of relationship between reverse drag shape ($\gamma$), listric fault shape ($\alpha_n$, $\alpha_{n-1}$) for minimalized hanging-wall shear ($S_{min}$). Graph based on eq (4).

*Blind normal fault* – The geometry of a *blind normal fault* is displayed in Figure 5. The fault is characterized by a blind end, without a lowermost detachment. Reverse drag is produced although the fault is planar. This is attained by layer parallel shear.

The shear necessary to create a blind normal fault ($S_N$) can be expressed by its fault dip $\psi$ and the axial angle $\gamma$ (Fig. 5). Similar to the previous derivation of $S$, $\Delta x$ is now the difference of the reverse drag bed length ($x$) and the undeformed bed length ($x'$) (Fig. 5).
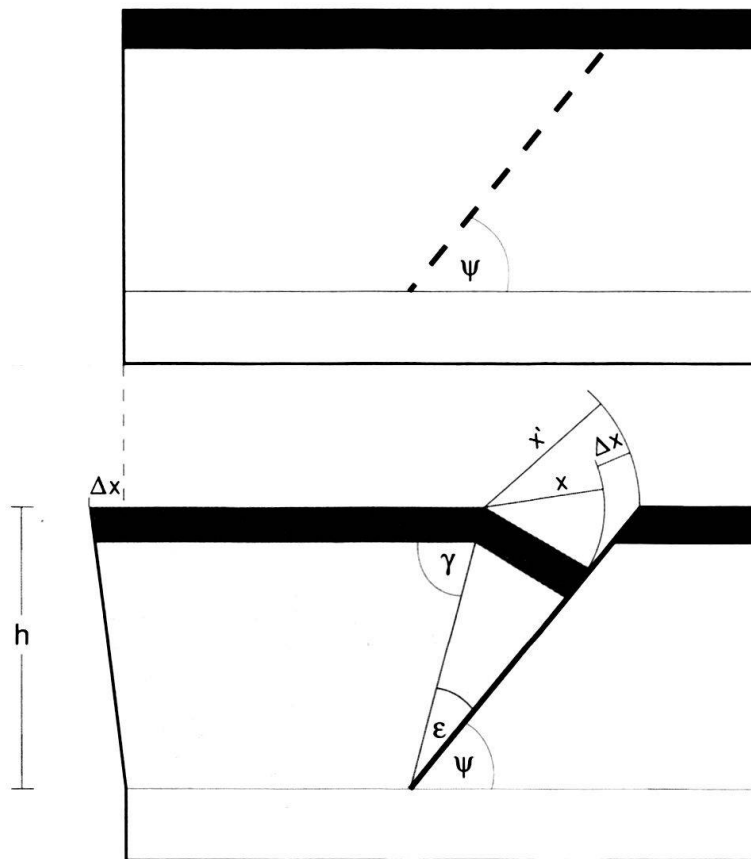
Fig. 5. Geometry of blind normal fault without basal detachment. The restored (top) and the deformed (bottom) section with the geometric relationships used to derive eq (8).

$$\Delta x = x - x' \tag{6}$$

The bed length $x$ and $x'$ are expressed by trigonometric functions in eq (6a) and (6b)

$$x = h \cdot \sin \varepsilon \cdot \frac{1}{\sin (\psi + 2\,\varepsilon)} \tag{6a}$$

$$x' = h \cdot \sin \varepsilon \cdot \frac{1}{\sin \psi} \tag{6b}$$

with $\varepsilon$ as the angle between the fault plane ($\psi$) and the axial surface ($\gamma$).

$$\gamma = \varepsilon + \psi \tag{7}$$

Inserting eqs (6a) and (6b) in eq (6) and dividing by $h$ leads to eq (8) which is graphically plotted in Figure 6.

$$S_N = \frac{\Delta x}{h} = \frac{\sin \varepsilon}{\sin (\psi + \varepsilon)} \cdot \left( \frac{1}{\sin (\psi + 2\,\varepsilon)} - \frac{1}{\sin \psi} \right) \tag{8}$$

After the Mohr-Coulomb criterion normal fault dips of 60° are expected (cf. SUPPE 1985). Field observations and laboratory experiments (HORSFIELD 1980) show often even steeper faults. However, such steep dips for blind normal faults lead only to little shear. For example a blind normal fault with a dip of 60° can have a maximum $S_N$ of $-0.05$ (Fig. 6) with $\varepsilon = 20$ and $\gamma = 80°$ respectively (cf. eq 7). The above expected $S_{min}$ for listric faults $(0.3 < S_{min} < 0.5)$ is about ten times larger. This discrepancy can be solved by stacking several blind faults (Fig. 7), which is equivalent to a simple addition of $S_N$ (cf. eq 5). The result of this structural stack is similar to a domino structure proposed by several authors to explain repetitive tilted block geometries in extended terrains (e.g. WERNICKE & BURCHFIELD 1982; VENDEVILLE & COBBOLD 1988).
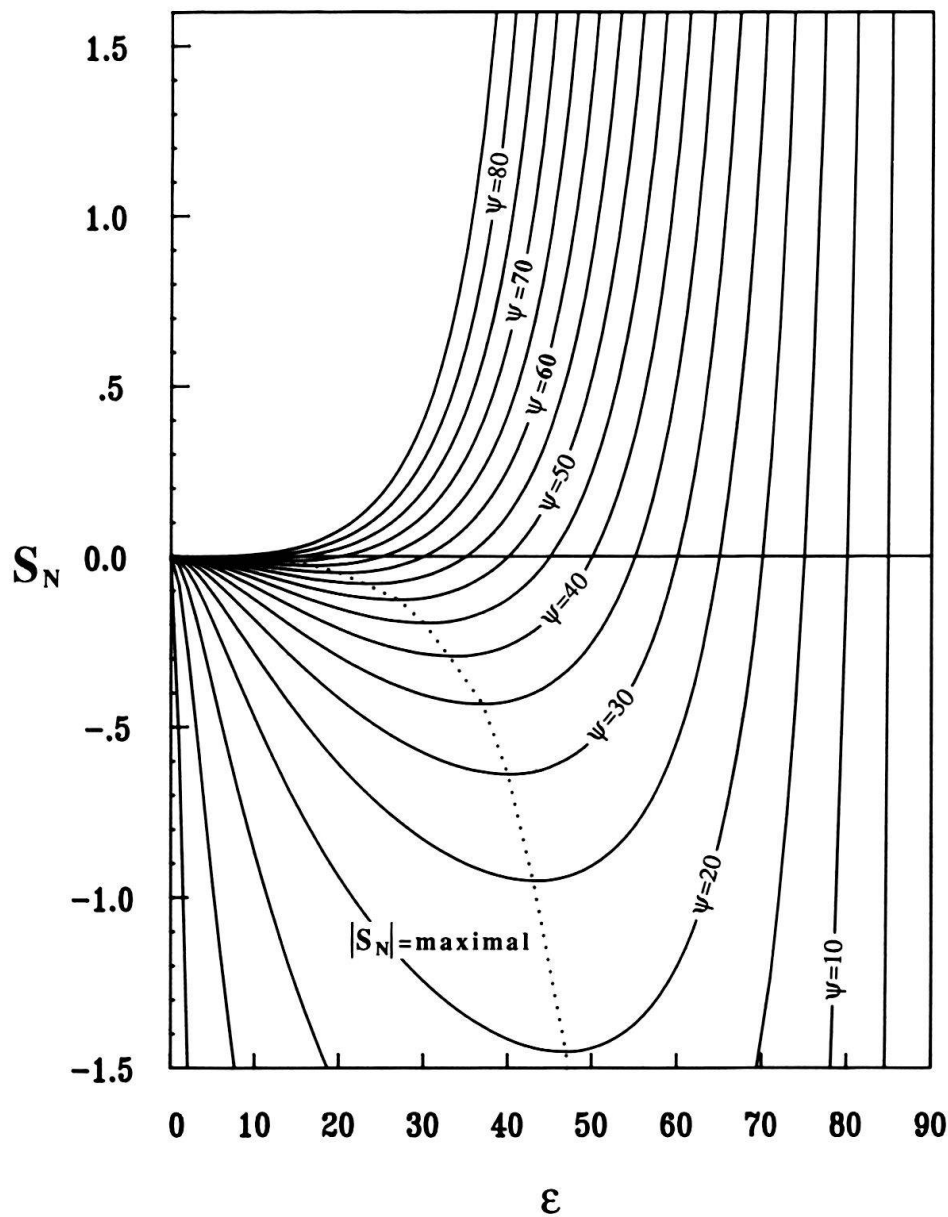


Fig. 6. Blind normal fault dips ($\psi$) and the necessary shear ($S_N$) to form a reverse drag, whereby $\varepsilon$ is the angle between the axial surface and the normal fault. Graph based on eqs (7) and (8).
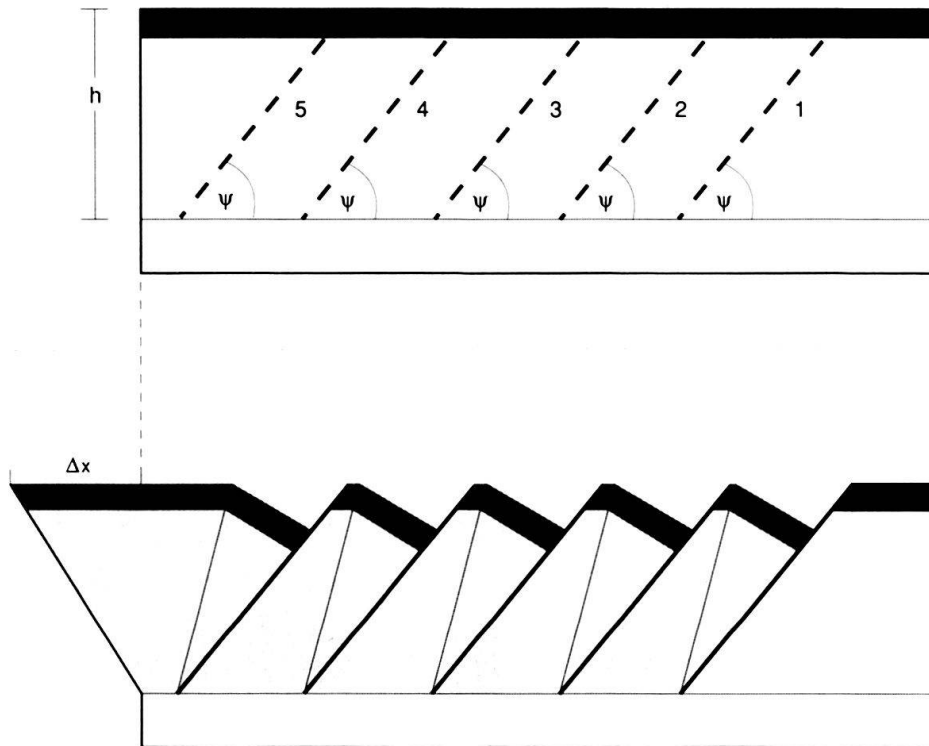
Fig. 7. Stack of five blind normal faults. The resulting structure is similar to a domino geometry.

*Blind grabens* – The geometry of a *blind graben* is shown in Figure 8. The pattern is similar to a full-graben (BALLY 1981). Such grabens are usually interpreted as crossing conjugate normal faults (ANDERSON 1951; HORSEFIELD 1980). Herein a different genesis of a full-graben is discussed. The main difference to the usual model is, that the space for the subsiding block is produced by simple shear, where the shear is restricted to the package of thickness $h$ (Fig. 8a, stippled area). Deformation is limited in depth, therefore the structure is referred as a blind graben. The shear $S_G$ necessary to create a blind graben is a function of the dip $\varphi$ of its edges. The relation for $S_G$ is expressed for a symmetric (Fig. 8a, eq 9) and a asymmetric (Fig. 8b, eq 10) blind graben.

$$S_G = 2 \tan (90 - \varphi) \tag{9}$$

$$S_G = \tan (90 - \varphi_1) + \tan (90 - \varphi_2) \tag{10}$$

The comparison of $S_G$ values with the above calculated $S_{min}$ values shows the same range of magnitude (for example: $\varphi = 60° \rightarrow S_G = 1.5$ or $\varphi = 70° \rightarrow S_G = 0.727$).

## Kinematics of half-graben deformation

In this paragraph a stepwise forward construction of half-graben models is discussed (Figs. 9 and 10). The restored section with the geometry of a pre-given listric fault is shown in Figure 9a. The listric fault is approximated by three fault-segments ($\alpha_2 = 65°$, $\alpha_1 = 30°$ and $\alpha_0 = 0°$). As a result of the extension about $e_1$ (Fig. 9b), the hanging-wall deforms due to the shape of the listric master fault as discussed above.
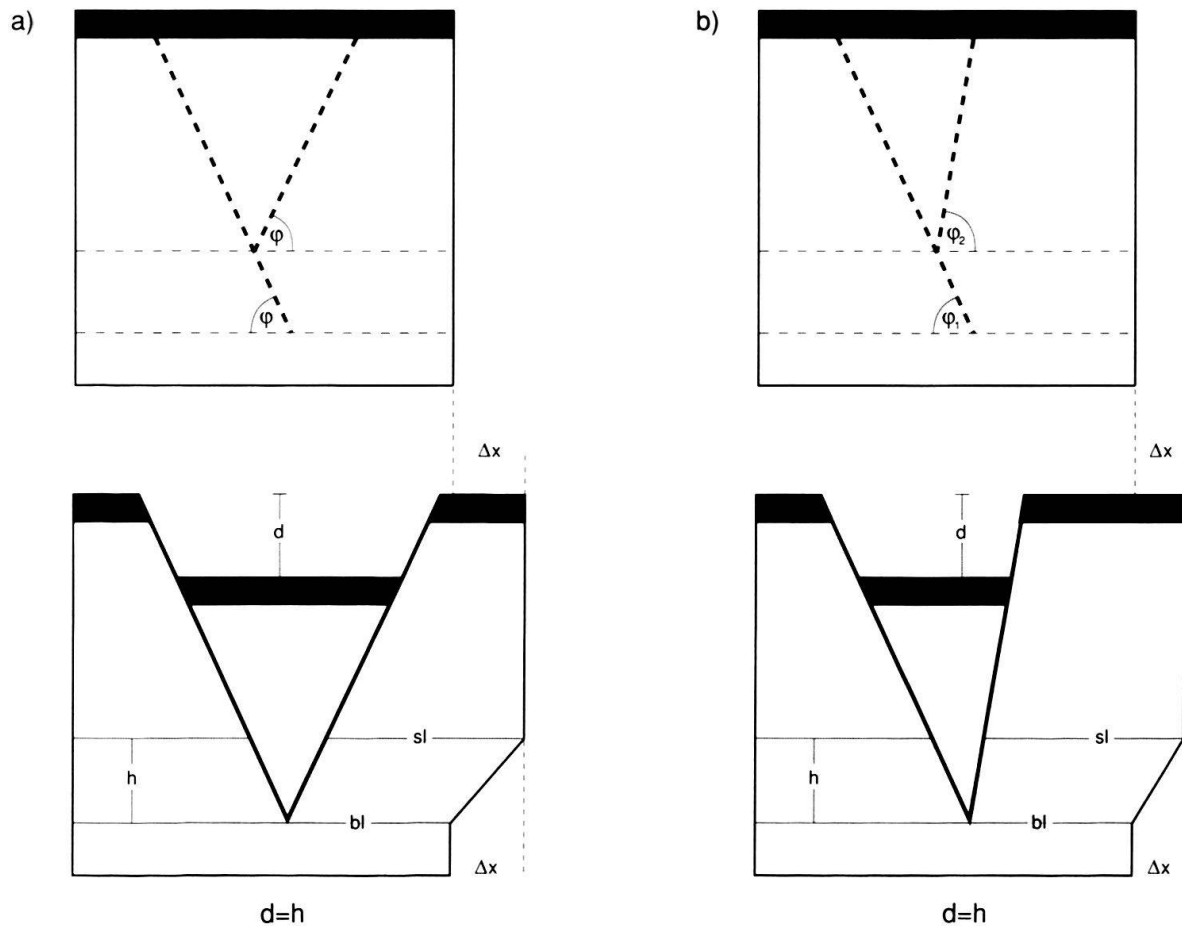
Fig. 8. Geometry of a symmetric (a) and an asymmetric (b) blind graben. The restored (top) and the deformed (bottom) section with the geometric relationships used to deriving eqs (9) and (10).

The geometry of the reverse drag ($\gamma_1$, $\gamma_2$) and the hanging-wall shear ($S_{min}$) can be calculated using equation (3) or read from Figure 4 ($\alpha_2 = 65°$, $\alpha_1 = 30° \rightarrow \gamma_1 = 69°$ $\rightarrow S_{min} = 0.625$; $\alpha_1 = 30°$, $\alpha_0 = 0° \rightarrow \gamma_1 = 60° \rightarrow S_{min} = 0.0$). The hanging-wall shear ($S_{min}$) which only affects the block gliding from the upper fault-segment onto the lower one, is compensated by a symmetric blind graben (Fig. 9b). The shape of this graben can be calculated using equation (9) ($S_{min} = 0.625 = S_G \rightarrow \phi = 72.6°$). According to the definition of a blind graben the subsidence ($d$) has to be equal to the thickness ($h$) of the sheared block. Furthermore the graben has to end at the lower level of the sheared block (cf. Fig. 8).

The section in Figure 9b is balanced. With further extension the reverse drag grows gradually and the existing secondary structure is transported with the hanging-wall. The old sheared block (Fig. 9b) remains inactive. But at its top shear starts to grow gradually upward. This creates a new unbalanced situation, which can only be solved by a new blind graben (Fig. 9c) as the old one can only grow downwards (cf. Fig. 8) which does not compensate the new shear. This mechanism of upwards growing simple shear and intermittent forming grabens continues until all layers cut off by the upper fault-segment are displaced onto the lower fault-segment or until extension ends (Figs. 9d and e).
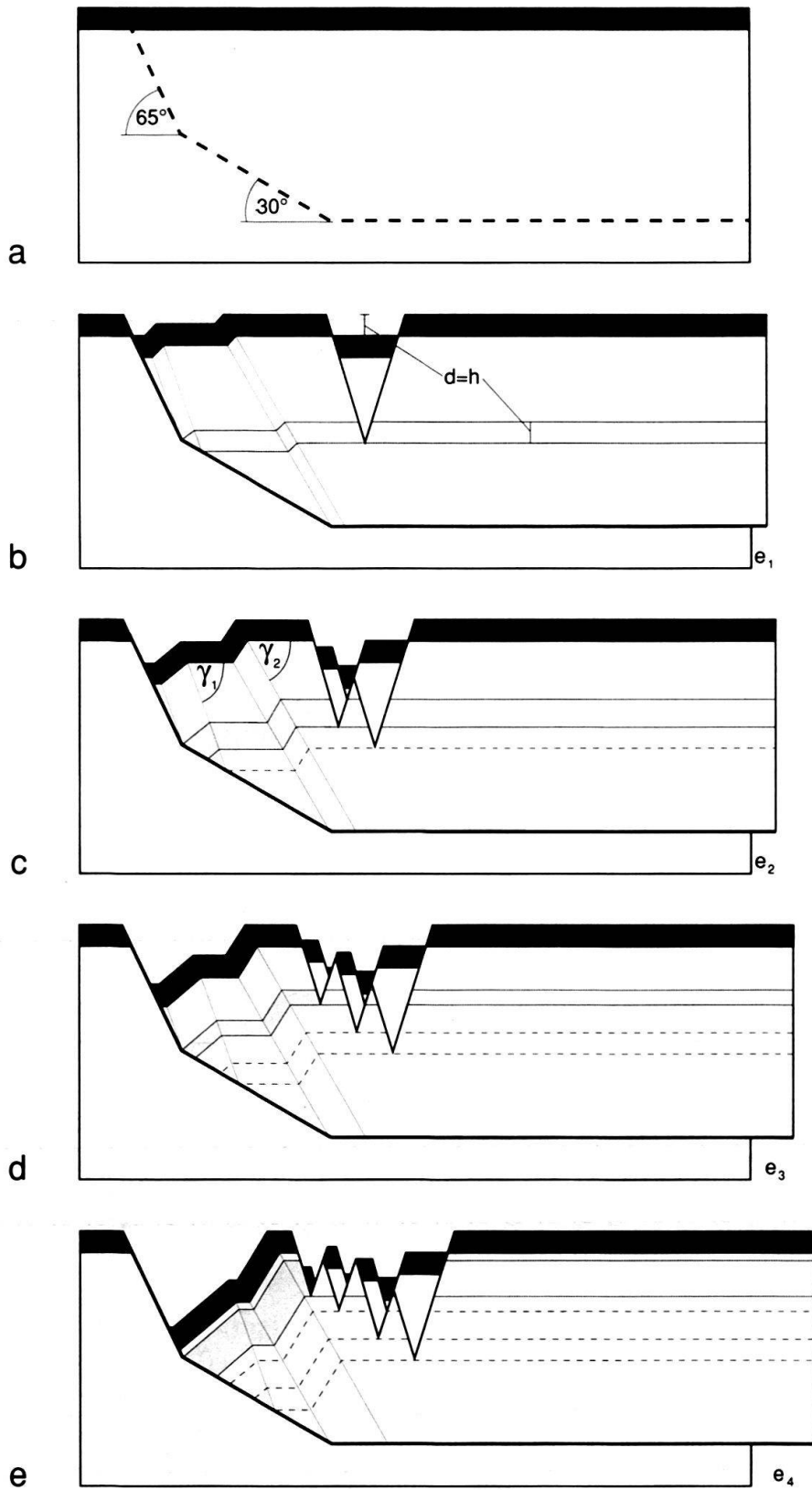
Fig. 9. Kinematic model of a half-graben structure. The listric fault is approximated by two fault-segments. Each kinematic step (a–e) is area and bed length balanced. Hanging-wall shear occurs only in the dashed layer packages and is compensated by blind grabens.
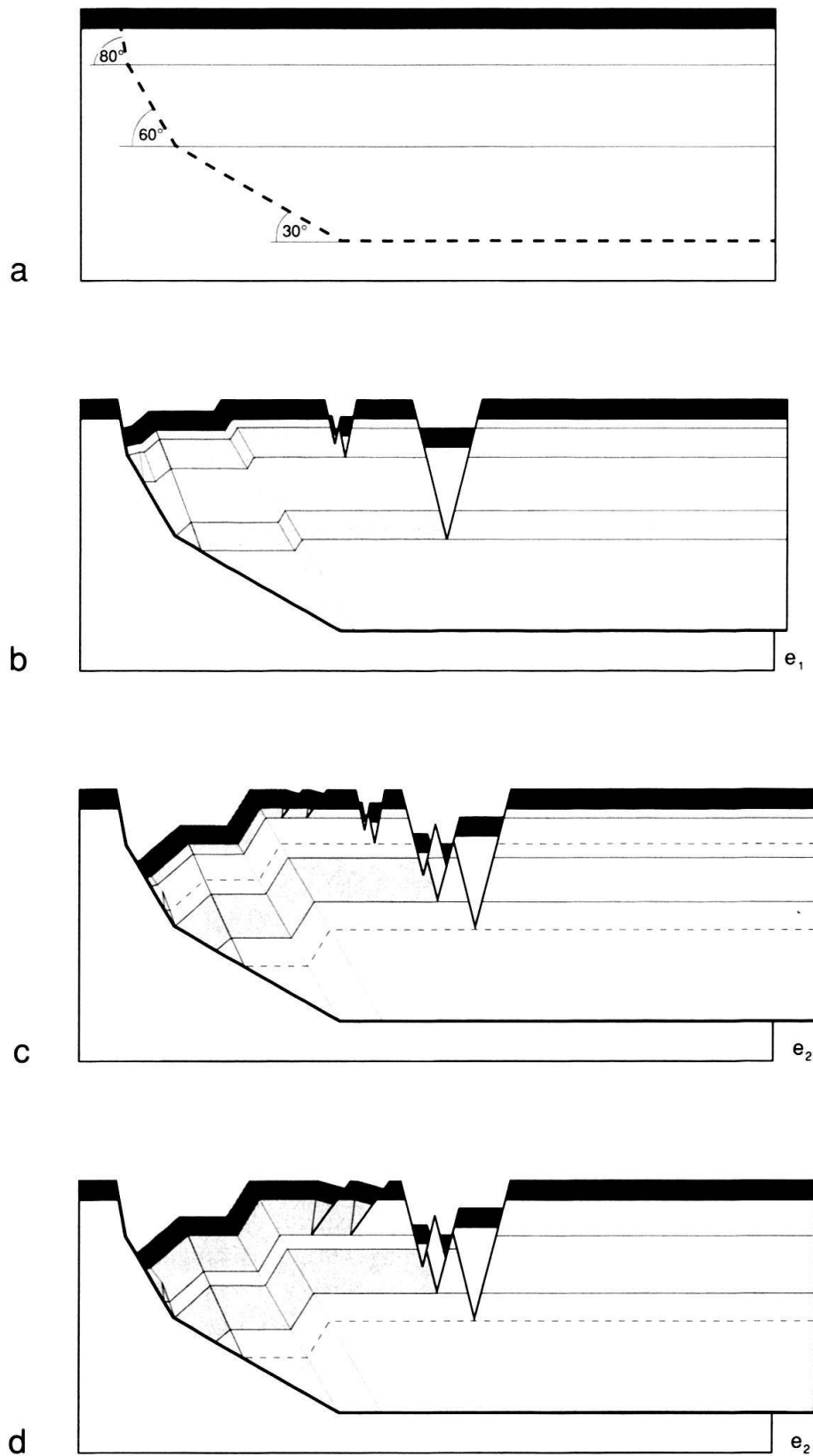
Fig. 10. Kinematic model of a half-graben structure. The listric fault is approximated by three fault-segments. Each kinematic step (a–d) is area and length balanced. Hanging-wall shear occurs only in the dashed layer packages and is compensated by blind grabens and by blind normal faults.

Figure 10 shows the same mechanism for the geometry of a four fault-segment example. In this system two levels of hanging-wall shear with secondary structures will be active. Blind grabens and also blind normal faults are used to balance the section. Figures 10c and 10d show the same extensional state, but different deformation in the upper shear level. Figure 10c is balanced with three secondary structures, whereas Figure 10d with only one. This demonstrates, that the presented strain calculations ($S_{min}$) allow the determination of the shape of secondary structures, but not the stage of deformation when they will form. This stage, as well as the thickness of the sheared package, is a function of stress.

The horizontal position of the secondary structures cannot be determined from calculations based on geometry. However, reasonable arguments can be presented to justify the chosen location in Figures 9 and 10. The intention is to keep the sheared block (stippled area in Figs. 9 and 10) as short as possible, which means that the secondary structure must form near to the cut-off of the listric fault. Also the first formed secondary structure must be the most distant from the cut-off because its unlikely that shear penetrates an existing fault. Finally, the construction (Figs. 9 and 10) avoids secondary structures that segment the reverse drag, so as to elude the complication of sheared fault geometries due to folding .

The kinematic sequence in Figures 9 and 10 show that deformation along the listric fault and the folding of the reverse drag might occur continuously. In contrast, the secondary structures form intermittent, and stay inactive if the corresponding hanging-wall shear is compensated. A conceivable mechanism is that stress grows in the sheared layers until local stress becomes greater than local stability. Then the secondary structures are formed and abruptly relax the stressed system. Such stress release is common in nearly all active rifts documented by subsiding blocks during earthquakes (e.g. JACKSON et al. 1982; JACKSON & McKENZIE 1983).

## Discussion

*Comparison with field observations* – Several seismic sections, for example in the Gulf Coast USA (BRUCE 1973; BALLY 1983), in the Niger Delta (MERKI 1972) or in Brunei (ELLENOR & JAMES 1984) reveal the above deduced geometry with a reverse drag and a sequence of secondary structures segmenting the hanging-wall. Blind ending structures have already been shown by CLOOS (1968) in the Golf of Tehuantapec (Mexico) and can also be recognized in the above referenced seismic sections.

GABRIELSEN (1984) interpreted a similar classification of extensional structures from structural maps of the Barents Sea. The author distinguished between first, second and third class structures. The first class structures are defined as regionally important features, reaching to greater depth and as having a longtime activity. The third class structures are only of local importance, usually shallower and with a shorter period of activity. The second class of structures is considered as an intermediate state between the other two classes.

*Application to sand-box experiments* – The sections in Figures 9 and 10 can be compared with sand-box experiments by ELLIS & McCLAY (1988). In these experiments alternating layers of sand and mica were used as medium for the hanging-wall. This medium was displaced over a pre-cut listric fault to study the hanging-wall defor-
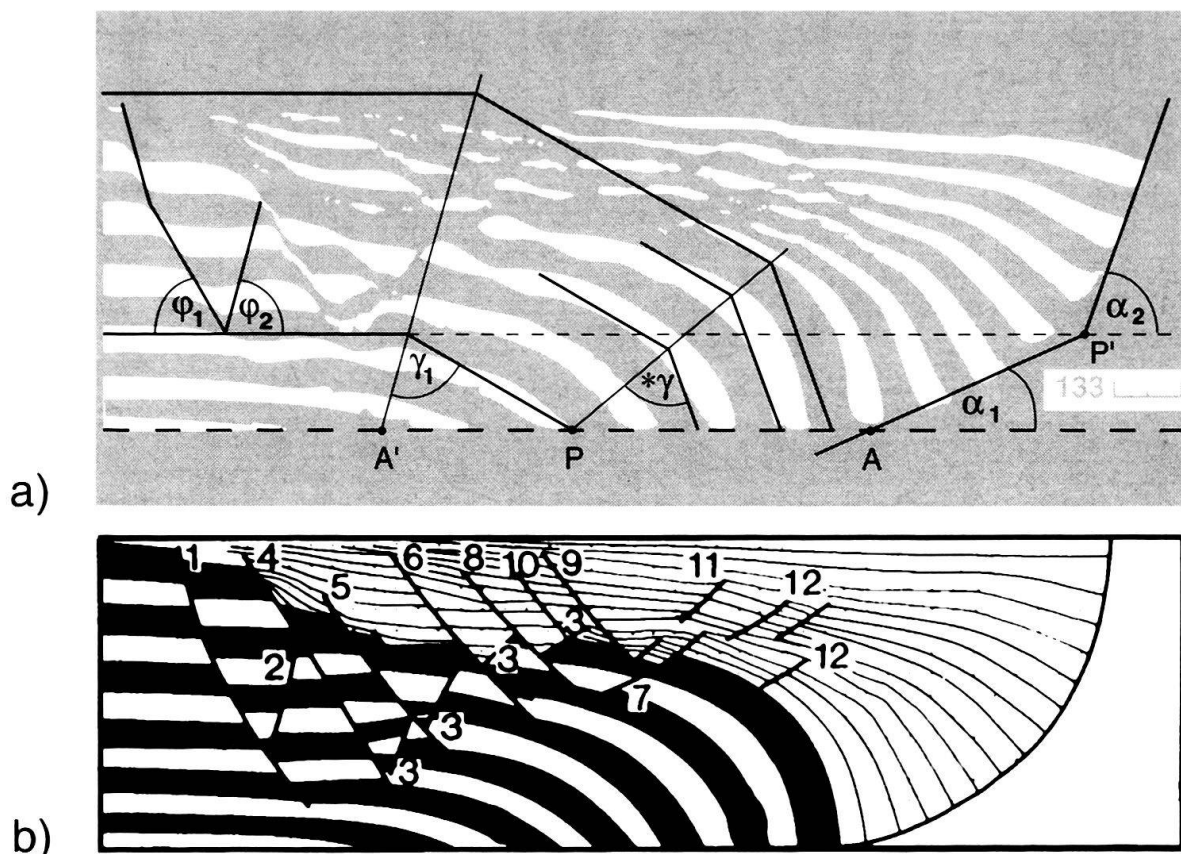
Fig. 11. a) Picture of sand-box experiment from Ellis & McClay (1988, experiment 133) overlaid by the calculated geometry. For explanations see text. b) Interpretation of the experimental results by Ellis & McClay (1988). Numbers correspond with time-dependent appearance of the faults.

mation. Two of their experimental results are shown in Figures 11b and 12b, respectively. The black and white layers represent the pre-rift rocks, whereas the lines show the geometry of the syn-rift sediments. The time-dependent appearance of single faults is shown by numbers on Figures 11b and 12b.

Phenomenologically the geometry of the experimental results corresponds to the constructions in Figures 9 and 10. The hanging-wall is folded by a reverse drag and segmented by secondary structures. The kinematic appearance of faults in the experiments accords with the constructed sections. One difference is that in the experiments the hanging-wall structures cut into the reverse drag and deform its fold shape. In the constructions this was avoided as to elude to complicate fault geometries. In all sand-box experiments full-grabens are dominant. No example for a two-level deformation as discussed in Figure 10 was found.

The derived geometric relation between listric fault, reverse drag and secondary structures is tested against these experiments (Figs. 11a and 12a). First the listric fault shape is calculated from the geometry of the secondary structures. Then the reverse drag is given by the listric fault shape. The depth of the change in dip of the listric fault (change from one fault-segment to the next) is defined as being at the base of the deepest secondary structure, which is the oldest (Figs. 10a and 11a; broken line). These structures are interpreted as full-grabens, defined by faults 1 and 2 (Fig. 11b) and by
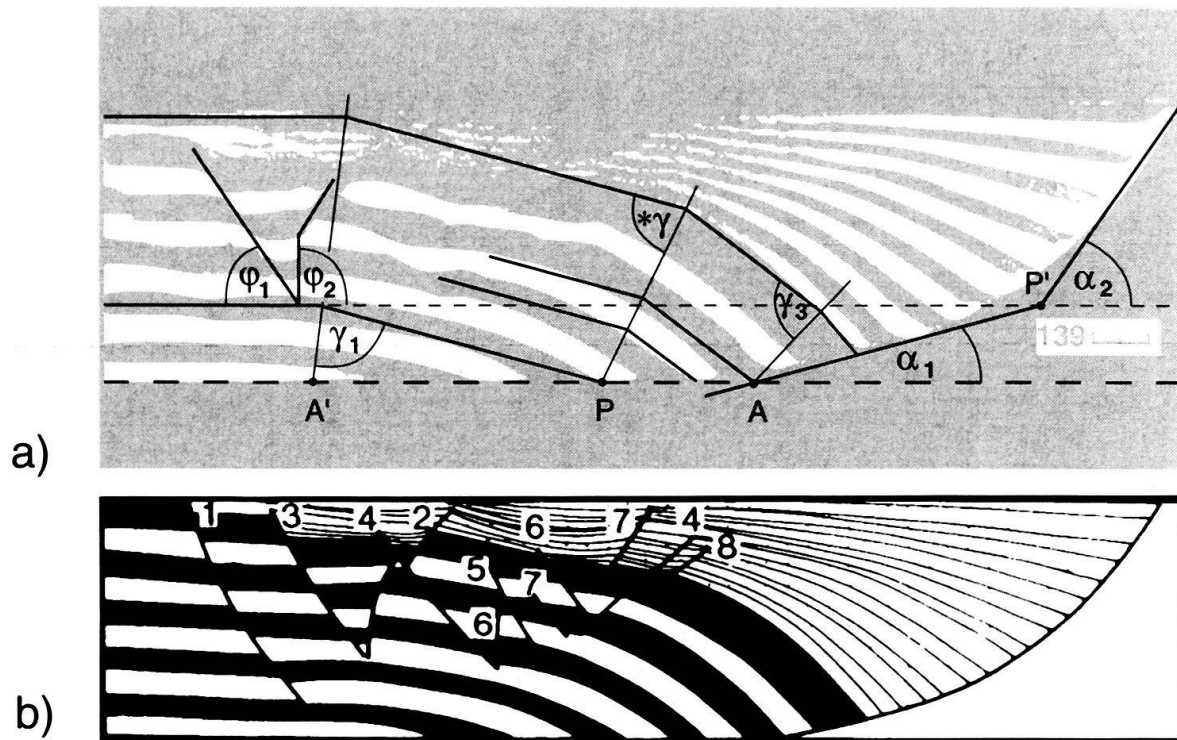
Fig. 12. a) Picture of sand-box experiment from ELLIS & McCLAY (1988, experiment 139) overlaid by the calculated geometry. For explanations see text. b) Interpretation of the experimental results by ELLIS & McCLAY (1988). Numbers correspond with time-dependent appearance of the faults.

faults 2 and 3 (Fig. 12b). In Figure 12b fault 1 can be interpreted as a blind normal fault. But it is neglected because the hanging-wall shear of a such steep blind normal fault is very small. The necessary shear to create the full-grabens can be determined by eq (10) (Fig. 11: $\varphi_1 = 60°$, $\varphi_2 = 75° \rightarrow S_G = 0.85$ and Fig. 12: $\varphi_1 = 55°$, $\varphi_2 = 90° \rightarrow S_G = 0.7$). If the hanging-wall shear ($S_G = S_{min}$) is known, several pairs of fault-segments are possible (Fig. 4). By choosing one of the fault-segments ($\alpha_n$ or $\alpha_{n-1}$) the other is uniquely defined. The dip of the upper fault-segment ($\alpha_2$) is determined graphically. Knowing $S_{min}$ and $\alpha_2$, the dip of the lower fault-segment ($\alpha_1$) and the axial angles ($\gamma_1$, $\gamma_2$) can be read from Figure 4 or determined with eq (3) (Fig. 11: $\alpha_2 = 70° \rightarrow \alpha_1 = 24°$ $\rightarrow \gamma_2 = 68°$ and with $\alpha_0 = 0° \rightarrow \gamma_1 = 75°$; Fig. 12: $\alpha_2 = 55° \rightarrow \alpha_1 = 15° \rightarrow \gamma_2 = 65°$ and with $\alpha_0 = 0° \rightarrow \gamma_1 = 82.5°$). The calculated lower fault-segment has to be placed at P', which is defined as the intersection of the upper fault-segment with the broken line (Figs. 11a and 12a).

The evaluation of the reverse drag needs further calculations, because beds cut off by the upper fault-segment were translated over the lower fault-segment onto the flat detachment. Therefore new fault dips ($*\alpha_n$, $*\alpha_{n-1}$) have to be determined. They can be calculated by adding the bed dip ($\beta$, defined by eq 4) to the old fault dips. The corresponding axial angle ($*\gamma$) can be read from Figure 4 or can be determined with eq (3) (Fig. 11: $*\alpha_n = 54°$, $*\alpha_{n-1} = 30° \rightarrow *\gamma = 70° \rightarrow S_{min} = 0.73$; Fig. 12: $*\alpha_n = 30°$, $*\alpha_{n-1} = 15°$ $\rightarrow *\gamma = (45°)$ or $79°$). The axial angle $\gamma_3$ in Figure 12 is determined graphically as the bisectrix between the bed dips defined by $*\gamma$ and by $\gamma_2$, respectively.
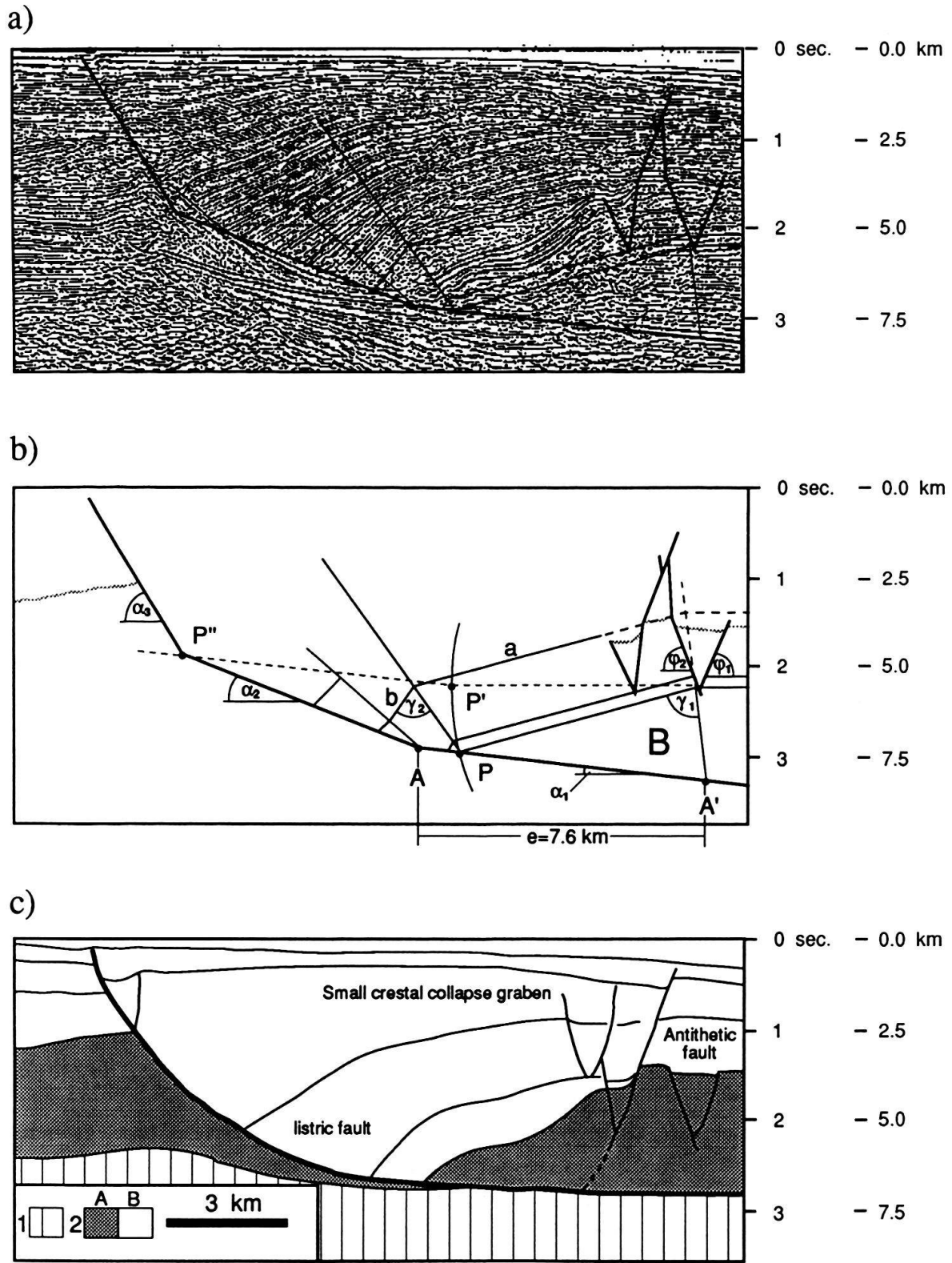
a)



b)



c)



Fig. 13. a) Seismic section published by FAURE & CHERMETTE (1989) overlaid by the calculated geometry. b) Construction of a balanced section using the seismic data. For explanations see text. c) Interpretation of the seismic data by FAURE & CHERMETTE (1989).

The calculated geometries (Figs. 11 and 12) are in good accordance with the experiments of ELLIS & McCLAY (1988). The constructed hanging-walls are a little too high compared to the experiments. This can be explained by secondary structures segmenting the reverse drag. A consequence is that the constructed beds are longer and therefore reach too high up.

*Application to seismic lines* – Unfortunately most published seismic sections are not depth-converted. Therefore the angular relationships between structures cannot easily be tested. However, a seismic section published by FAURE & CHERMETTE (1989; no regional reference) was used to test the proposed balancing method (Fig. 13). The vertical scale of this seismic section is slightly stretched to receive an equal scale geometry. The assumed mean seismic velocity is 5 km/s.

A difference to the sand-box experiments is that the lowermost fault-segment is not flat. The slight subsidence of the hanging-wall beds compared to the foot wall beds sustains the lack of a flat detachment in Figure 13a. Furthermore, the seismic reflectors between A and A' show a slight dip. In order to balance the section this dip is considered to be the dip of the lowermost fault-segment ($\alpha_1$). From the seismic data, however, this dip has been determined to be $\alpha_1 = 6°$.

Two bed dips are read directly from the seismic data (Fig. 13b; lines a and b). The bisectrix between this beds defines the axial surface ($\gamma_2 = 70°$). With $\gamma_2$ and $\alpha_1$ the dip of the second fault-segment ($\alpha_2 = 20°$) is calculated using eq (3). The intersection of the axial surface ($\gamma_2$) with the lowermost fault-segment (P) defines the tip of the block B, which was cut off by the second fault-segment ($\alpha_2$). The blind end of the right hand graben defines the upper limit of this block (Fig. 13b; broken line). From the intersection of this block limit with the beds cutting through P the first axial surface ($\gamma_1 = 83°$) is constructed. The dips of the graben faults read from Figure 13a and eq (10) were used to define the hanging-wall shear ($\varphi_1 = 70°$, $\varphi_2 = 72° \rightarrow S_G = S_{min} = 0.69$). With $S_{min}$ and $\alpha_2$ the third fault-segment dip ($\alpha_3 = 58°$) is read from Figure 4. The intersection of the third and the second fault-segment (P'') is found by restoring block B (see construction in Fig. 13b; P → P' → P'').

The constructed geometry of the listric fault and the hanging-wall beds coincides well with the seismic data. The undulating layers in the reverse drag of the pre-rift sediments show a discrepancy from the model calculation (Fig. 13a). This might be explained by earlier deformation of the layers.

The seismic data show that the blind grabens migrate into higher stratigraphic levels and towards the main fault as suggested by the model proposed. Furthermore, the subsidence of the first graben is equal to the difference in depth to the second graben. All these observations give strong evidence for the occurrence of blind grabens within rift systems (cf. Figs. 6, 9 and 10). In addition the amount of extension (*e*) along the listric fault which is defined as the distance between *A* and *A'* (Fig. 13; *e*= 7.6 km) can be evaluated using the geometrical model developed in this paper.

## Conclusions

1. The proposed model describes a relation between the shape of a listric/planar master fault and the geometry of the corresponding hanging-wall. Hanging-wall bed lengths are conserved by the introduction of simple shear.

2. The compensation of shear with extensional structures leads to a hierarchical classification of structures in extensional systems with *primary* and *secondary* structures.

3. Primary structures defined as half-grabens are the regionally important features. Secondary structures defined as *blind grabens* and *blind normal faults* are of local importance only and do not contribute to the amount of regional extension.

4. The geometry of the secondary structures depends on the geometry of the primary structures ($S_{\text{hanging-wall}} = -S_{\text{secondary}}$).

5. Primary structures deform continually during extension. In contrast secondary structures are active only during a short period and cannot be reactivated during the same extensional phase.

6. New secondary structures end in higher stratigraphic levels than the previous ones.

7. A sequence of secondary structures develops opposite to extension direction towards the reverse drag.

The above model calculations and construction technique can be used as a powerful tool for the interpretation of structural and seismic data in extensional terrains.

## Acknowledgments

## REFERENCES

ANDERSON, E.M. 1951: The dynamics of faulting and dyke formation. Oliver and Boyd, London.

BALLY, A.W. 1981: Atlantic type margin. In: Geology of passive margins: History, structure and sedimentological record (Ed. by BALLY, A.W.). Amer. Assoc. Petroleum Geol. Education Course Note Series 19, 1.1–1.48.

— 1982: Musings over sedimentary basin evolution. Philos. Trans. r. Soc. London 305, 325–338.

— 1983: Seismic expression of structural styles. Amer. Assoc. Petroleum Geol. Studies in Geology, 15, 2.

BALLY, A.W., BERNOULLI, D., DAVIS, G.A. & MONTARDERT, L. 1981: Listric normal faults. Ocean. Acta, Paris, Actes 26. Congrès International de Géologie. Colloque géologie des marges continentales. Paris, 7.–17. juillet 1980, 87–101.

BOYER, S.E. & ELLIOT, D. 1982: Thrust-systems. Amer. Assoc. Petroleum Geol. Bull. 66, 1196–1230.

BRUCE, C.H. 1973: Pressure shale and related sediment deformation: mechanism for fault development of regional contemporaneous faults. Amer. Assoc. Petroleum Geol. Bull. 57, 878–886.

BRUN, J.P., CHOUKROUNE, P. & FAUGERE, E. 1985: Les discontinuités significatives de l'amincissement crustal. Bull. Soc. géol. France 8, 139–144.

CLOOS, E. 1968: Experimental analysis of Gulf Coast fracture patterns. Amer. Assoc. Petroleum Geol. Bull. 52, 402–444.

COBBOLD, P.R. 1983: Kinematic and mechanical discontinuity at a coherent interface. J. Struct. Geol. 5, 341–349.

DE CHARPAL, O., GUENNOC, O., MONTARDERT, L. & ROBERTS, D.G. 1978: Rifting crustal attenuation and subsidence in the Bay of Biscaya. Nature 275, 706–811.

EATON, G.P. 1982: The Basin and Range Province: Origin and tectonic significance. Ann. Rev. Earth Planet Sci. 10, 409–440.

ELLENOR, D. & JAMES, D.M.D. 1984: The oil and gas resources of Brunei. In: The geology and hydrocarbon resources of Negra Brunei Darussalem, Kota Batu, Muzim Brunei (Ed. by JAMES, D.M.D.) 103–139.

ELLIS, P.G. & McCLAY, K.R. 1988: Listric extensional fault systems – results of analogue model experiments. Basin Research 1, 55–70.

FAUGERE, E. & BRUNE, J.P. 1984: Modélisation expérimentale de la distension continentale. C. r. Acad. Sci. (Paris) 299, 365–370.

FAURE, J.L. & CHERMETTE, J.C. 1989: Deformation of tilted blocks and extension measurements. Bull. Soc. géol. France 8, 461–476.

GABRIELSEN, R.H. 1984: Long-lived fault zones and their influence on the tectonic development of the south western Barents Sea. J. geol. Soc. (London) 141, 651–662.

GANS, G.P., MILLER, E.L., McCARTHY, J. & OULDCOTT, M.L. 1985: Tertiary extensional faulting and evolving ductile-brittle transition zones in the northern Snake Range and vicinity: New insights from seismic data. Geology 13, 189–193.

GEISER, P.A. 1988: The role of kinematics in the construction and analysis of geological cross-sections in deformed terranes. In: Geometries and Mechanisms of Thrusting with special references to the Appalachians (Ed. by MITRA, G. & WOIJTAL, S.). Spec. Pap. geol. Soc. Amer. 222, 47–76.

GIBBS, A.D. 1983: Balanced cross-sections construction from seismic sections in areas of extensional tectonics. J. Struct. Geol. 5, 153–160.

–     1984: Structural evolution of extensional basin margins. J. geol. Soc. (London) 141, 609–620.

GROSHONG, R.H. (JR.) 1989: Half-graben structures: Balanced models of extensional fault-bend folds. Bull. geol. Soc. Amer. 101, 96–105.

HAMBLIN, W.K. 1965: Origin of "reverse drag" on the downthrown side of normal faults. Bull. geol. Soc. Amer. 76, 1145–1164.

HORSFIELD, W.T. 1980: Contemporaneous movement along crossing conjugate normal faults. J. Struct. Geol. 2, 305–310.

JACKSON, J. & McKENZIE, D. 1983: The geometrical evolution of normal fault systems. J. Struct. Geol. 5, 471–482.

JACKSON, J.A., GAGNEPAIN, J., HOUSEMAN, G., KING, G.C.P., PAPADIMITRIOU, P., SOUFLERIS, C. & VIRIEUX, J. 1982: Seismicity, normal faulting and the geomorphological development of the Gulf of Corinth (Greece): the Corinth earthquakes of February and March 1981. Earth and plan. Sci. Lett. 57, 377–397.

KLEMPERER, S.L. 1988: Crustal thinning and nature of extension in the northern North Sea from deep seismic reflection profiling. Tectonics 7, 803–821.

LAUBSCHER, H.P. 1965: Ein kinematisches Modell der Jurafaltung. Eclogae geol. Helv. 58, 231–318.

LE PICHON, X. & SIBUET, J.C. 1983: Passiv margins: A model of formation. J. geophys. Res. 86, 3708–3720.

MERKI, P. 1972: Structural geology of Cenocoic Niger delta. In: African Geology. (Ed. by DESSAUVIAGIE, T.F.J. & WHITEMAN, A.J.). Ibadan University, 635–646.

PROFFETT, J.M. 1977: Cenozoic geology of the Yerington district, Nevada, and implications for the nature and origin of Basin and Range faulting. Bull. geol. Soc. Amer. 88, 247–266.

ROSENDAHL, B.R. 1987: Architecture of continental rifts with special reference to east Africa. An. Rev. Earth Planet. Sci. 15, 445–503.

ROWAN, M.G. & KLIGFIELD, R. 1989: Cross-section restoration and balancing as aid to seismic interpretation in extensional terrains. Amer. Assoc. Petroleum Geol. Bull. 73, 955–966.

SUPPE, J. 1983: Geometry and kinematics of fault bend folding. Amer. J. Sci. 283, 684–721.

–     1985: Principles of Structural Geology. Prentice-Hall, Inc., Englewood, New Jersey.

VENDEVILLE, B. & COBBOLD, P.R. 1988: How normal faulting and sedimentation interact to produce listric fault profiles and stratigraphic wedges. J. Struct. Geol. 10, 649–659.

VENDEVILLE, B., COBBOLD, P.R., DAVY, P., BRUN, J.P. & CHOUKROUNE, P. 1987: Physical models of extensional tectonics at various scales. In: Continental extensional tectonics. (Ed. by COWARD, M.P., DEWEY, J.F. & HANCOCK, P.L.). Spec. Publ. geol. Soc. (London), Oxford 28, 95–107.

VERALL, P. 1981: Structural interpretation with application to North Sea problems. Course notes No. 3, Joint Ass. Petr. Expl. Courses (UK).

WERNICKE, B. & BURCHFIELD, B.G. 1982: Modes of extension tectonics. J. Struct. Geol. 4, 105–115.

WHITE, N.J., JACKSON, J.A. & McKENZIE, D.P. 1986: The relationship between the geometry of normal faults and that of the sedimentary layers in their hanging-walls. J. Struct. Geol. 8, 897–909.